Structural Engineering and Mechanics, Vol. 6, No. 5 (1998) 485-496
DOI: http://dx.doi.org/10.12989/sem.1998.6.5.485

Modeling interply debonding in laminated architectural glass subject to low velocity impact

F.W. Flocker† and L.R. Dharani‡

Department of Mechanical and Aerospace Engineering and Engineering Mechanics, University of Missouri-Rolla, Rolla, MO 65409-0050, U.S.A.

Abstract. Standard finite element wave propagation codes are useful for determining stresses caused by the impact of one body with another; however, their applicability to a laminated system such as architectural laminated glass is limited because the important interlayer delamination process caused by impact loading is difficult to model. This paper presents a method that allows traditional wave propagation codes to model the interlayer debonding of laminated architectural glass subject to low velocity, small missile impact such as that which occurs in severe windstorms. The method can be extended to any multilayered medium with adhesive bonding between the layers. Computational results of concern to architectural glazing designers are presented.

Key words: debonding; impact; laminated glass; fracture; finite element method.

1. Introduction

Laminated architectural glazing, similar to that found in automotive "safety glass," is constructed by placing an adhesive polymeric interlayer between two soda-lime glass plies. Polyvinyl butyral (PVB) is the industry standard interlayer because of its adhesive and optical qualities. The purpose of the interlayer is to prevent the glass plies from shattering on impact thereby greatly reducing the possibility of injury caused by sharp pieces of flying glass.

In architectural applications, low velocity, small missile impact is usually due to windborne debris such as roof gravel which can be hurled with sufficient velocity to break windows. Beason, Meyers and James (1984) did a study of damage to window glass in Houston, Texas caused by Hurricane Alicia which struck Houston in 1983. In that study, significant window damage was reported for a localized area of downtown Houston. The primary cause of window damage was windborne roof gravel. Because Alicia was a relatively mild hurricane, the need for improved impact resistance was apparent in order to be better prepared for the possibility of even stronger hurricanes that may strike.

In their work, Beason, Meyers and James (1984) reported that the outside ply of a laminated unit can serve as an impact shield. Their design methodology allows the outside ply to fracture but not the inside ply. If the inside ply also fractures, window strength is significantly reduced to the point where wind and/or heating, ventilating and air conditioning loads can cause rapid collapse of the window. The building interior is thus exposed to the

† Currently with Stress Engineering Services, Houston, TX
‡ Professor

outside weather, greatly increasing the possibility of damage to the building contents, injury to people, and disruption of normal business activity. An impact resistant design that fractures only at the outer ply preserves building envelope integrity and can be replaced at the convenience of the building owner with minimal disruption of occupant activities. It should be noted that this sacrificial ply concept requires that the inside ply itself be of sufficient strength to withstand design wind loading.

One objective of this work is to present a method whereby traditional finite element wave codes can be used to model low velocity, small missile impact in laminated architectural glass when interlayer delamination must be included in the analysis. A secondary objective is to investigate the effect of interlayer delamination on critical stresses in the laminate. It is well known that the amount of delamination is a parameter that can be varied in order to optimize the performance of automotive windshields (Huntsberger 1981). Limited debonding results in a more compliant structure that can absorb more energy, thereby reducing the chance of injury should a passenger impact the windshield during a collision. Excessive debonding can allow the undesirable event of a passenger completely penetrating the windshield. Here, it is determined if controlled delamination can also optimize architectural glazing with respect to small missile, low velocity impact resistance.

2. Formulation of the impact problem

Fig. 1 shows the idealized impact problem under consideration. A typical three layer glazing system is considered: two soda-lime glass plies separated by a PVB interlayer. The system is impacted by a hard missile modeled as a chromium steel ball with initial impact velocity v_0. A "worst case" scenario to simulate windborne roof gravel during a hurricane is assumed: the normal impact of a 7.94 mm (5/16 inch) diameter steel ball at 35.8 m/s (80 mph).

Cylindrical coordinates (r, z, θ) as shown in Fig. 1 with a Lagrangian description of motion are used to formulate the problem. A condition of torsionless axisymmetry is assumed so that normal stresses are independent of the angle θ and the shear stress components $\tau_{r\theta}$ and $\tau_{z\theta}$ vanish. The impact problem is solved numerically using a modified version of the large scale

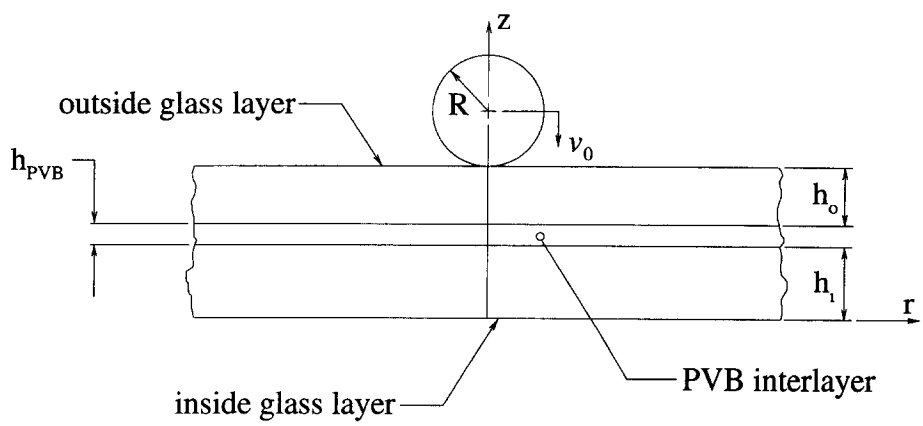

Fig. 1 Sketch of the problem studied: glass/PVB/glass laminate subjected to impact by a spherical ball

explicit finite element code DYNA2D (Whirley *et al.* 1992). The code incorporates two main modifications that allow the simulation of this impact problem. The first code modification involves a cracking algorithm to model glass fracture under low velocity impact. A detailed discussion of the cracking algorithm is given in a previous work (Flocker and Dharani 1997a) and a brief review is given below. The second code modification is a method to model the delamination process. The details of the delamination algorithm will be presented below.

The steel ball and inside glass ply are modeled as linear elastic materials. The outside glass ply is modeled as linear elastic with cracking. The PVB interlayer is a viscoelastic polymer modeled as a so-called standard linear solid. Many polymers follow this linear viscoelastic law very well especially when strains are small (Fung 1965) as in the case of laminated glass subject to low velocity impact. Details of the material models as well as determination of the various material properties are presented in a previous work (Flocker and Dharani 1997b).

2.1. The computational crack model

The crack model is based on the work of Flocker and Dharani (1997a). There, it was shown that of the four main types of cracks that form when glass is impacted by a spherical projectile (cone, median, lateral and radial (Knight *et al.* 1977, Cook and Pharr 1990)), the so-called cone crack is of primary concern in this situation with the others being nonexistent or having negligible affect on the stress of concern. As will be explained in more detail, the stress of concern is the maximum principal stress located at the innermost surface of the inside glass layer directly beneath the impact site (see Fig. 1). A typical cone crack with cone angle ϕ formed in a brittle material after an impact from a spherical projectile of radius R is shown in Fig. 2(a). It was shown that for practical architectural glazing systems, the cone crack completely penetrates the outside ply when subjected to the worst case impact scenario studied here. Fig. 2(b) illustrates a cone crack formed in the outside layer of a typical laminated architectural glass unit. Because this type of crack is axisymmetric, a plug forms in the outside glass ply and is driven against the PVB interlayer resulting in high stress concentrations in the PVB interlayer at the edge of the cone.

A propagating cone crack is modeled in a finite element mesh as follows: at the appropriate time and location, an element "cracks" by setting deviatoric stresses and hydrostatic tension

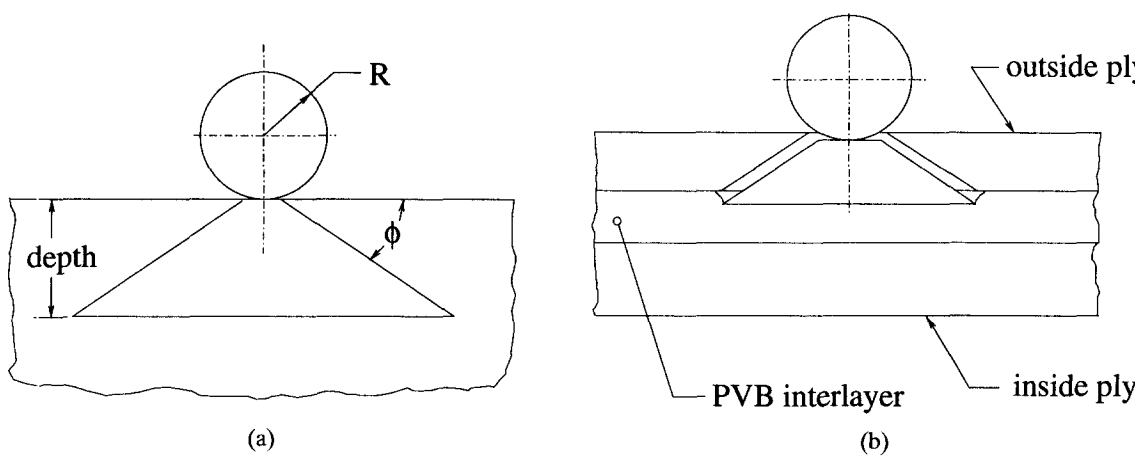

Fig. 2 Cone crack in an infinite half-space and a laminated glass unit. (a) Cone crack and geometry in an infinite half-space. (b) Penetrating cone crack in a laminated glass unit

to zero. If, in subsequent time steps, deviatoric stresses are computed to be other than zero, they are reset to zero. Similarly, if hydrostatic tension is computed, it is reset to zero. Hydrostatic compression is unaffected in a cracked element. Thus, a cracked element will not support shear or tension but will support compression. The determination of the appropriate time and location for elements to crack is based on the observation that the geometry and speed of a propagating cone crack are well defined for the problem under consideration (Flocker and Dharani 1997a). The crack starts at the impact surface just outside the contact patch of the projectile as shown in Fig. 2(a). Crack initiation is between 0.62 μs and 1.5 μs after contact is made between the projectile and surface. The crack then propagates through the outside glass ply at a nearly constant speed of 1550 m/s and at a cone angle $\phi = 30^{\circ}$.

2.2. The interface debonding model

The interface debonding model is based on the primary assumption that debonding is a propagating phenomenon. Debonding starts and then progresses away from an initial location. The point of initiation is assumed to be where the cone crack meets the PVB interface because, as will be shown, this is where stresses are very high. Fig. 2(b) (exaggerated) illustrates the initiation of debonding.

Debonding of the PVB interlayer and glass is a form of peeling (Huntsberger 1981). Initial debonding occurs at a high peel angle with subsequent debonding changing rapidly to low angle peel. Kaelble (1959) analyzed the mechanics of peel adhesion and found that at high peel angles, cleavage forces dominate at the point of debonding (tip of the debonded region) while at low peel angles, shear forces dominate. Here, the term "cleavage force" means a force that acts normal to the debonding interface while "shear force" refers to a force acting parallel to the debonding interface. Thus, debonding can occur if a critical shear stress (τ_{rz}) or a critical cleavage stress (tensile σ_z) is exceeded at the debonding interface. Fig. 3 shows the location where debonding initiates. In this figure, "*X's*" are used to denote "cracked" elements forming a portion of the cone crack while the "*O*" denotes the element where debonding initiates. Subsequent debonding along the interface occurs in a progressive manner when critical stresses are exceeded.

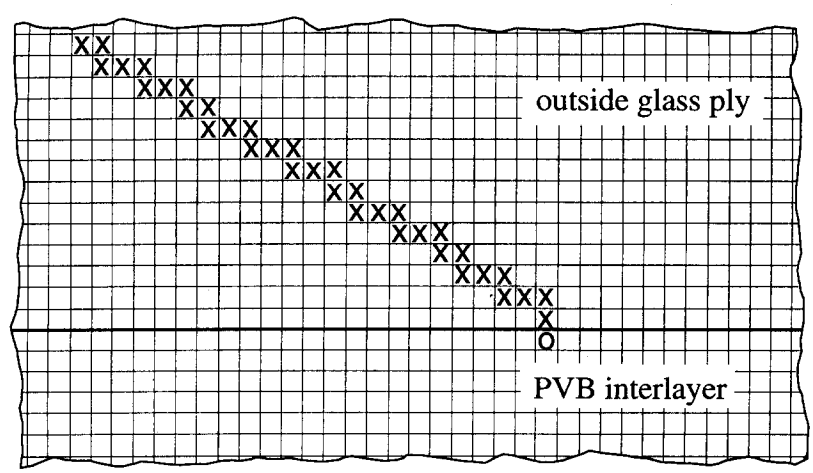

Fig. 3 Illustration of the location of the initiation of debonding

Interface debonding is modeled in the same manner as element cracking. That is, once interface stresses in a PVB element reach the debonding criterion, element stresses are relaxed by setting deviators and hydrostatic tension to zero. In subsequent time steps, if deviators or hydrostatic tension are computed other than zero, they are reset to zero. Hydrostatic compression is unaffected. Thus, the debonded region cannot support shear or tension but can support compression. To minimize the thickness of the debonded region (theoretically, infinitesimally thin), stress relaxation occurs only in one side of the interface, in this case, the glass side.

The determination of appropriate debonding stress measures is now discussed. It is assumed that a suitable debonding criterion can be based on the values of interface shear stress and axial tensile (cleavage) stress at the tip of the debonding region since shear and cleavage forces are of primary concern in the steady state peel mechanism (Kaelble 1959). It is further assumed that the two are related. Intuitively, one would expect that less shear is required to debond a strip of adhesive from a substrate if a tensile force exists between the two. The relationship between shear and cleavage stress at the point of debonding can be conveniently determined from plane strain peel tests at various peel angles ranging from 0° to 90° At 90° peel, only cleavage stress exists; while at some low angle of peel, only shear stress exist. At other peel angles, both stress components are present.

The mechanics of the peel test are described in detail by Kaelble (1959, 1960). Briefly, a strip of adhesive with a flexible backing is applied to a rigid substrate as illustrated in Fig. 4. A peel force, P, is applied to the flexible backing at peel angle ω. The force required to strip the adhesive from the backing is then measured. Both the peel angle and peel rate can be varied, but are usually held constant for a particular test. The cleavage and shear stresses at the location of the debonding interface are denoted by σ_0 and τ_0, respectively, and are given by Kaelble (1960) as.

$$\sigma_0 = 2\beta P(\beta m_c + \sin\omega) \tag{1}$$

$$\tau_0 = \alpha P \cos\omega \tag{2}$$

where ω is the peel angle and P is the peel force per unit width (see Fig. 4). The terms α, β and m_c are given by

$$\alpha = \left(\frac{G}{2Eah}\right)^{1/2} \tag{3}$$

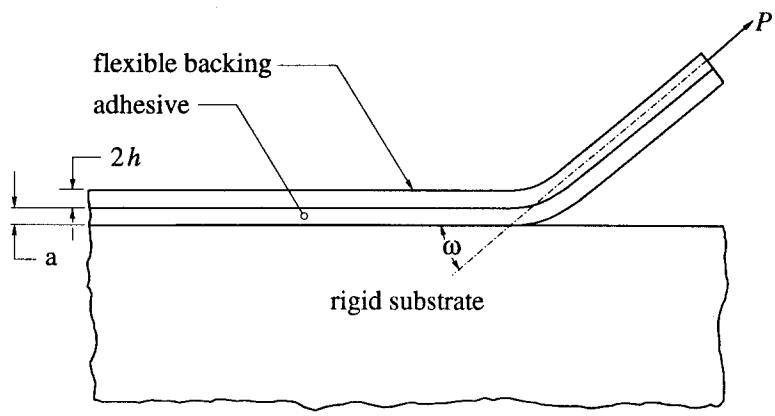

Fig. 4 Illustration of the plane strain peel test

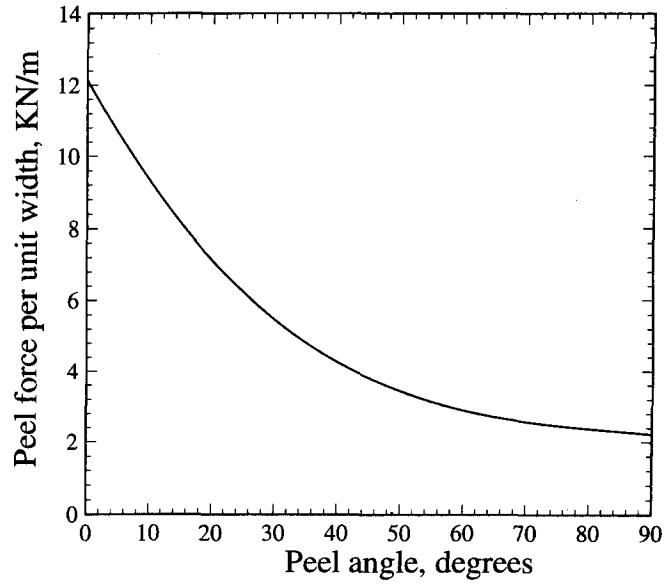

Fig. 5 Example plot of peel force as a function of peel angle

$$\beta = \left(\frac{3Y}{8Ea\ h^3} \right)^{1/4} \tag{4}$$

$$m_c = \left[\frac{4E\ h^3 (1-\cos\omega)}{3P} \right]^{1/2} - h\ \cos\omega \tag{5}$$

where G and Y are, respectively, the shear and Young's moduli for the adhesive, E is Young's

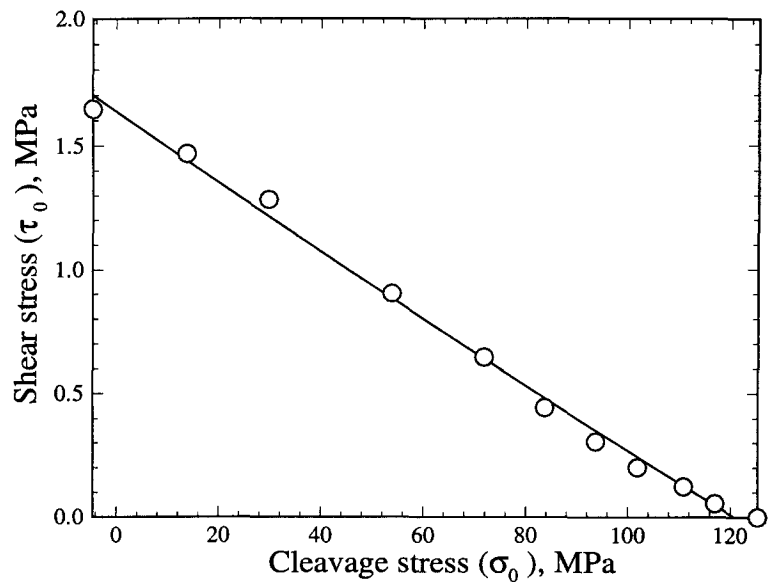

Fig. 6 Plot of interface cleavage stress versus interface shear stress at the point of debonding

modulus for the flexible backing, a is the adhesive thickness and $2h$ is the flexible backing thickness. By varying the peel angle and measuring the peel force, a series of peel tests will provide the required relation between σ_0 and τ_0.

The determination of a debonding criterion is best illustrated with a hypothetical yet representative example. The following values are assumed: Y=2.57 GPa, G=1.0 GPa, E=70 GPa, a=0.76 mm, $2h$=1.0 mm. It is further assumed that high rate peel testing of PVB bonded to a glass substrate yields the peel force versus peel angle graph shown in Fig. 5. The next step is to plot σ_0 and τ_0 for peel angles between 0° and 90° σ_0 and τ_0 are obtained from Eqs. (1) and (2) using data from Fig. 5. The result is shown in Fig. 6 where the data points are obtained from the hypothetical data of Fig. 5. Here, a linear relation seems adequate to describe debonding shear stress as a function of cleavage stress.

For the case where a linear relationship exists between σ_0 and τ_0, it is useful to define the following terms. Let σ_{cut} denote the debonding cleavage stress when no shear is present. Similarly, let τ_{cut} denote the debonding shear stress when no cleavage stress exists. Then the shear stress required for debonding is given by

$$\tau_0 = \tau_{cut} - \left(\frac{\tau_{cut}}{\sigma_{cut}}\right)\sigma_0 \tag{6}$$

σ_{cut} is found using Eq. (1) with 90° peel test data. To determine τ_{cut}, the peel angle where cleavage stress is zero must first be determined. Let ω^* denote this angle. From Eq. (1) it can be seen that this requires $\beta m_c + \sin\omega^* = 0$ or, using Eq. (5):

$$\beta\left\{\left[\frac{4Eh^3(1-\cos\omega^*)}{P}\right]^{1/2} - h\cos\omega^*\right\} + \sin\omega^* = 0 \tag{7}$$

ω^* is usually near 0° where a suitable approximate function for $P(\omega)$ can be obtained from Fig. 5. Using the approximate $P(\omega)$ in Eq. (7), ω^* can be found numerically and then τ_{cut} is found from Eq. (2). For the illustrative example considered here, ω^*=1.22° σ_{cut}=126 MPa and τ_{cut}= 1.62 MPa.

If one accepts beforehand the linear relation of Eq. (6), a great simplification in experimental work can be realized. By substituting Eqs. (4) and (5) into Eq. (1) evaluated at ω=90° one can get, after some manipulation

$$\sigma_{cut} = 2P\left(\frac{3Y}{8Ea}\right)^{1/4}\left[\left(\frac{2YE}{3a\,P_{90}^2}\right)^{1/4} + h^{-3/4}\right] \tag{8}$$

where P_{90} denotes the value of P at 90° peel. For practical experimental setups, the second term in the square brackets of Eq. (8) is small compared with the first, resulting in

$$\sigma_{cut} \approx \left(\frac{2Y\,P_{90}}{a}\right)^{1/2} \tag{9}$$

Thus, σ_{cut} is approximately dependent only on the adhesive thickness, elastic modulus and 90° peel force per unit width. In addition, using Eqs. (2) and (3) at $\omega \approx 0°$ results in

$$\tau_{cut} \approx P_0 \left(\frac{G}{2Eah} \right)^{1/2} \tag{10}$$

where P_0 is the value of P at very low peel angle. The result is a good approximation of Eq. (6) based on only two peel tests, one at 90° and the other at very low angle. For the example considered here, approximate values for σ_0 and τ_0 of 126 MPa and 1.67 MPa, respectively are obtained, which compare favorably to those obtained above.

The finite element debonding logic is thus: if an element at the tip of the debonded zone experiences a cleavage stress greater than or equal to σ_{cut}, it debonds. If the cleavage stress is less that σ_{cut}, the element can still debond if its shear stress exceeds a value predicted by Eq. (6). For example, if the cleavage stress at the element coinciding with the tip of the debonded region is 20 MPa, then a shear stress of 1.35 MPa or greater in the element will cause it to debond.

3. Finite element computations

The geometry of a typical architectural glazing unit is considered. With reference to Fig. 1, h_0=4.76 mm, h_{PVB}=1.59 mm, h_i=6.35 mm. Fig. 7 shows the finite element mesh which, because of the problem axisymmetry, represents only half of the actual geometry. The bold lines in the figure are used to show the three layers of the laminate. Boundaries *c-d* and *b-e* are unconstrained. Boundary *a-b-c* is the symmetry axis. Boundary *d-e* is a so-called "nonreflecting boundary" that is achieved by producing an impedance matching function that cancels incoming stress waves so that none are reflected back from the boundary. Nonreflecting boundaries are used to simulate infinite bodies, in this case an infinite laminate of finite thickness. The mesh is similar to one used successfully in a previous work (Flocker and Dharani 1997a). The projectile mesh is identical, whereas the target mesh has been extended to allow debonding away from the impact site. The uniform portion of the target mesh is the same as used before, the nonuniform mesh is the extended portion.

The concern is mainly with stresses at the surfaces of the glass plies since this is where cracks tend to open and extend under tensile loading (Knight *et al.* 1977, Chaudhri and

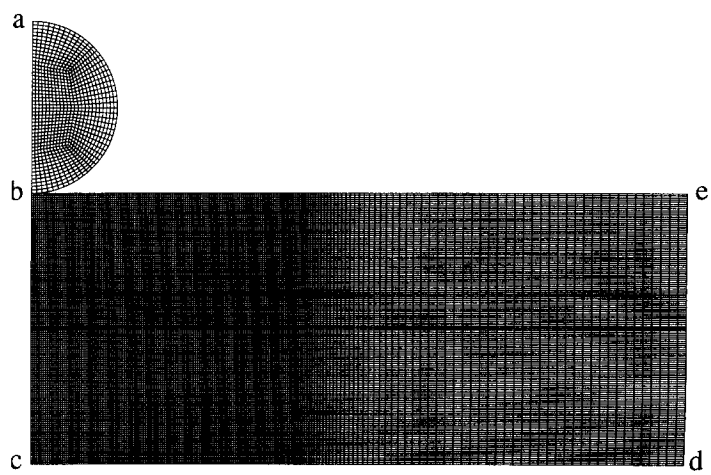

Fig. 7 Finite element mesh used for the computations

Walley 1978, Frank and Lawn 1967, Chaudhri and Kurkjian 1986). Furthermore, since the design methodology of Beason *et al.* (1984) assumes that the outside ply is sacrificed to the incoming missile, concern is restricted to surface stresses in the inside glass ply since this is the ply that must not fracture. In other words, one need not be concerned with surface stresses in the outside ply since they are assumed high enough to cause fracture; however, one needs to be concerned with surface stresses in the inside ply since they should be below that required to initiate fracture. As shown previously (Flocker and Dharani 1997a, 1997b), the critical location for inside ply crack initiation is element 1 of the mesh located at the innermost surface along the line of symmetry (point *c* in Fig. 7). In addition, it was shown that the coordinate system adopted here coincides with the principal directions of element 1 and that the maximum tensile principal stress in element 1 is the stress measure of concern since it corresponds to a mode I crack opening stress for a surface crack located normal to the surface. Therefore, the main interest in this work is the effect of interlayer debonding on element 1 maximum tensile principal stress.

4. Results

Fig. 8 shows the effect of the cone crack on PVB/glass interface stresses. The stress values shown are maximum values for each PVB interface element occurring over the entire impact cycle. While this figure does not show the stress distribution for any particular instant in time, it is useful in illustrating the high shear and normal stresses produced in the PVB near where the cone crack meets the interface. It is these high stresses that lead to interlayer delamination.

To determine the effect of interlayer debonding, the amount of debonding was varied from none to nearly the entire interface for the mesh of Fig. 7. This was accomplished by reducing the value of τ_{cut}. Three particular cases that illustrate the general trend are discussed. The three cases are illustrated in Fig. 9. Case A (Fig. 9a) has only the cone crack; σ_{cut} and τ_{cut} were set high enough that no debonding occurs. Case B has a limited amount of debonding as shown in Fig. 9b. Case C (Fig. 9c) shows the extreme case of debonding. In these illustrations, the debonding shown is the maximum extent produced over the impact cycle. The time history of

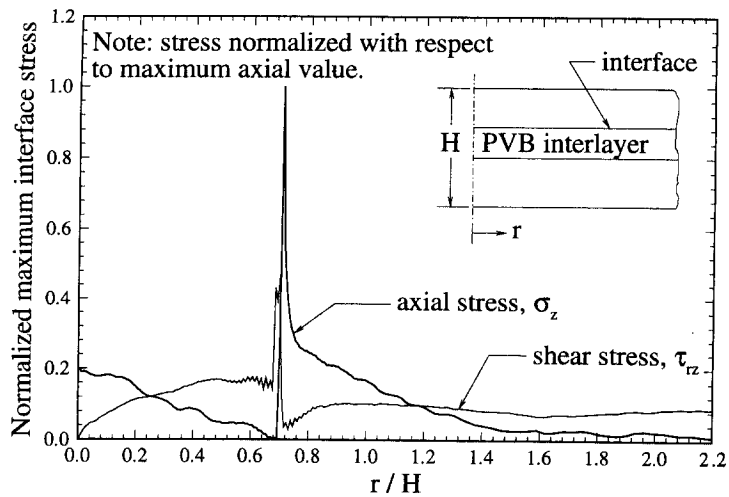

Fig. 8 Illustration of stress concentrations produced by a penetrating cone crack

cracking and debonding for Case C is shown in Fig. 10, where the crack is shown to progress through the outside glass ply. In this sequence of figures, v_0 is the initial impact velocity and v is the velocity at the time indicated. The crack is shown to form at around 2 μs and has progressed approximately two thirds of the way through the outside glass ply at 5 μs. The crack impinges on the PVB interface at about 7.6 μs. As shown, only a small amount of debonding has occurred by 10.8 μs when the projectile comes to rest prior to rebounding. It is seen that most of the debonding occurs during the restitution phase of the impact.

To determine the effect of interlayer debonding on overall impact resistance of the system requires time history plots of the maximum principal stress for the critical location (element 1) of the mesh. Fig. 11 shows the stress cycle imposed on the critical element for each case of

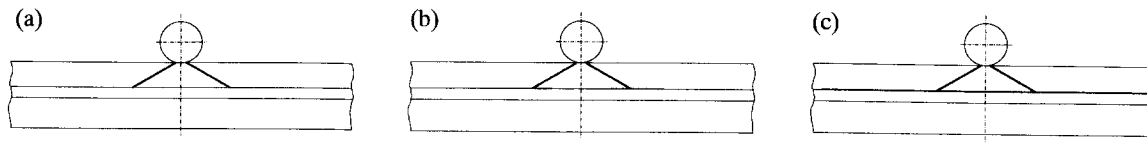

Fig. 9 (a) Debonding Case A. No interface debonding. (b) Debonding Case B. Limited interface

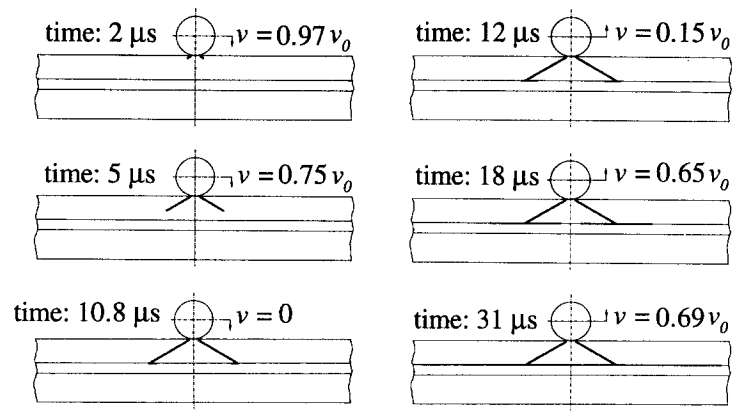

Fig. 10 Cracking and debonding time history for Case C

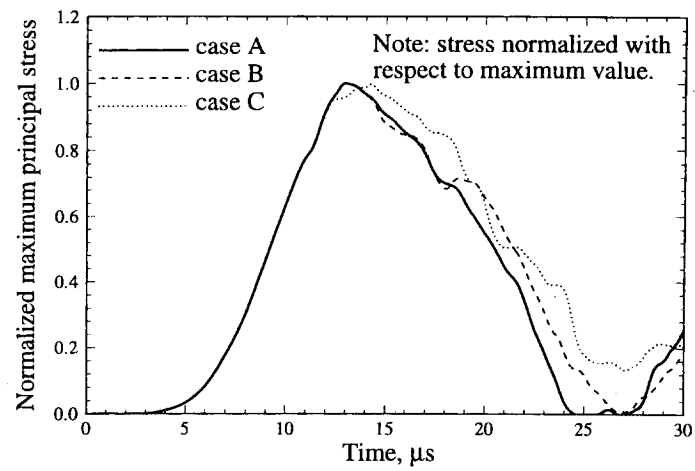

Fig. 11 Critical element stress pulse shapes for debonding Cases A, B, C

Fig. 9. The tendency for a crack in the critical element to open and extend under impact loading can be quantified through a dynamic stress intensity factor (Grady 1985, Freund 1973):

$$K_I(a_c, t) = \sqrt{\pi a_c} \int_0^t \frac{d\sigma(s)}{ds} f\left[\frac{c_s(t-s)}{a_c}\right] ds \tag{11}$$

where K_I is the dynamic mode I stress intensity factor, a_c is a characteristic crack dimension, c_s is the shear wave speed, σ is the stress applied to the crack (in the case studied here, maximum principal stress) and the function $f[c_s(t\text{-}s)/a_c]$ depends on the type of crack. A crack exposed to a higher dynamic stress intensity factor is more inclined to open and propagate than another crack in the same material subject to a lower dynamic stress intensity factor. From Eq. (11), with the derivative of the stress function in the integrand, one can see that it is the shape of the stress pulse prior to reaching its maximum value that determines if a crack will extend. Portions of the stress pulse with positive slope (positive derivative) add to the dynamic stress intensity factor, while portions of the pulse with negative slope reduce the dynamic stress intensity factor. After the maximum stress value, the derivative of the stress function turns generally negative resulting in a lower dynamic stress intensity factor as given by Eq. (11). Therefore, if the crack has not extended by the time the pulse reaches its peak, it will not extend at all. An inspection of Fig. 11 shows very little difference in the stress pulse shapes prior to their maximum values for the three debonding cases considered here. One can conclude that, for the three cases considered here, debonding has little affect on the tendency of a crack to open and extend.

5. Conclusions

A method is presented that allows traditional finite element wave propagation codes to model adhesive debonding in layered media. An illustrative example applied to the case of laminated architectural glass was applied, although the finite element algorithm is general to other layered media and to concentric cylinder models of fiber composites. The only restriction on the use of the algorithm is that an interface stress debonding criterion be applied. The algorithm provides an analytical tool that can be used to significantly reduce expensive and time consuming laboratory testing.

An illustrative example of the debonding model was applied to a typical architectural glazing unit in order to determine if a controlled amount of debonding is beneficial with respect to low velocity, small missile impact. Because debonded laminated architectural glass provides a potential safety hazard (debonded glass pieces can break off and hit pedestrians), it is important that the debonding process be incorporated into computational programs that simulate windborne debris impact.

Debonding was shown to have negligible effect on the resistance of inner ply fracture to small, windborne debris impact. It is noted that this is in contrast to automotive glazing in which debonding is a parameter that can be optimized in order to reduce the possibility of injury should a passenger or driver impact the windshield during a collision (Huntsberger 1981). Therefore, in the sacrificial ply example considered, with nothing to be gained through controlled debonding, the adhesive bond between the PVB interlayer and glass plies should be made as strong as possible in order to minimize the hazard of debonded glass pieces coming loose.

Acknowledgements

This work was supported by the U. S. National Science Foundation, the Missouri Department of Economic Development Through Manufacturing Research and Training Center, du Pont, Inc. and the Monsanto Chemical Company.

References

Beason, W.L., Meyers, G.E. and James, R.W. (1984). "Hurricane related window glass damage in Houston", *J. of Structural Engineering*, **110**(12), 2843-2857.

Chaudhri, M.M. and Kurkjian, C.R. (1986). "Impact of small steel spheres on the surfaces of 'normal' and 'anomalous' glasses", *J. Am. Ceram. Soc.*, **69**(5), 404-410.

Chaudhri, M.M. and Walley, S.M. (1978). "Damage to glass surfaces by the impact of small glass and steel spheres", *Phil. Mag. A*, **37**(2), 153-165.

Cook, R.F. and Pharr, G.M. (1990). "Direct observation and analysis of indentation cracking in glasses and ceramics", *J. Am. Ceram. Soc.*, **73**(4), 787-817.

Ferry, J.D., *Viscoelastic Properties of Polymers*, John Wiley and Sons, New York, 1961.

Flocker, F.W. and Dharani, L.R. (1997a). "Modeling fracture in laminated architectural glass subject to low velocity impact", *J. Matls. Sci.*, **32**, 2587-2594.

Flocker, F.W. and Dharani, L.R. (1997b). "Modeling stress wave propagation in laminated glass subject to low velocity impact", *Engineering Structures*, **19**(10), 851-856.

Frank, F.C. and Lawn, B.R. (1967). "On the theory of Hertzian fracture", *Proc. Roy. Soc.*, **A299**, 291-306.

Freund, L.B. (1973). "Crack propagation in an elastic solid subjected to general loading_III. stress wave loading". *J. Mech. Phys. Solids*, **21**, 47-61.

Fung, Y.C. (1965). *Foundations of Solid Mechanics*, Prentice-Hall, Englewood Cliffs, NJ, 20-28.

Grady, D. (1985). "The mechanics of fracture under high-rate stress loading", in *Mechanics of Geomaterials*, Z. Bazant, ed., John Wiley and Sons, Chichester, 129-156.

Huntsberger, J.R. (1981). "Adhesion of plasticized poly (vinyl butyral) to glass", *J. Adhesion*, **13**, 107-129.

Kaelble, D.H. (1959). "Theory and analysis of peel adhesion: mechanisms and mechanics", *Trans. Soc. Rheo.* III, 161-180.

Kaelble, D.H. (1960). "Theory and analysis of peel adhesion: bond stresses and distributions", *Trans. Soc. Rheo.* IV, 45-73.

Knight, C.G., Swain, M.V. and Chaudhri, M.M. (1977). "Impact of small steel spheres on glass surfaces", *J. Matl. Sci.*, **12**, 1573-1586.

Whirley, R.G., Englemann, B.E. and Halquist, J.O. (1992). "DYNA2D, a nonlinear, explicit, two-dimensional finite element code for solid mechanics", user manual, Lawrence Livermore National Laboratory Report, UCRL-MA-110630.